Journal of Alloys and Compounds 656 (2016) 729–734

Contents lists available at ScienceDirect

Journal of Alloys and Compounds

journal homepage: http://www.elsevier.com/locate/jalcom

Composition design of high B_s Fe-based amorphous alloys with good amorphous-forming ability

Anding Wang [a, b], Chengliang Zhao [a, b], Aina He [a, b], He Men [a, b], Chuntao Chang [a, b, *], Xinmin Wang [a, b]

[a] Key Laboratory of Magnetic Materials and Devices, Ningbo Institute of Materials Technology and Engineering, Chinese Academy of Sciences, Ningbo, Zhejiang 315201, China
[b] Zhejiang Province Key Laboratory of Magnetic Materials and Application Technology, Ningbo Institute of Materials Technology and Engineering, Chinese Academy of Sciences, Ningbo 315201, China

ARTICLE INFO

Article history:
Received 11 September 2015
Received in revised form
23 September 2015
Accepted 24 September 2015
Available online 30 September 2015

Keywords:
Fe-based amorphous alloy
High B_s
Soft magnetic properties
Amorphous-forming ability

ABSTRACT

The composition design rules for high B_s amorphous alloys are introduced from the binary phase diagram, atomic size and the effects of amorphous forming elements on magnetic performance and ribbon manufacturability. The effects of metalloid elements on amorphous-forming ability and magnetic properties as well as origin of the excellent properties for high Fe content $Fe_{83}(Si,B,P,C)_{17}$ amorphous alloys are explored. Based on the similar Fe content of Fe–B, Fe–P and Fe–C eutectic alloys, the alloy systems with the combination of Fe, B, P, C and Si are beneficial to the achievement of high B_s and amorphous-forming ability. With the addition of Si, P and C in $Fe_{83}B_{17}$, the amorphous-forming ability and the soft-magnetic properties improve clearly. The critical wheel speed decrease from 54 m/s to 12 m/s and the maximum thickness increase to 76 μm. The improvement of the amorphous-forming ability is discussed in term of the competition effect and the eutectic theory.

1. Introduction

Soft-magnetic materials play important functional role in electronic and magnetic products which greatly affect the human production and living ways. In the 21st century, stronger, lighter, higher energy efficient and more silent are the long-term targets and key challenges of device development [1]. This requires constant enhancement of magnetic performance containing higher effective permeability (μ_e) and saturation flux density (B_s), lower coercivity (H_c) and core loss. After a centennial development, many kinds of soft magnetic materials have been developed and some have been widely used in different fields according to their unique performance [2]. Fig. 1 shows relationship between μ_e at 1 kHz and B_s for the representative soft magnetic materials. Among these materials, silicon steels and ferrites still dominate the markets. Although lower in B_s and effective permeability than metallic materials, their far higher resistivity continue to make ferrites advantageous for medium–high frequency applications which are unlikely to be supplanted, particularly above 1 MHz [3]. However, for the widest used silicon steels, the dominate positions in electricity generation, transmission and transformation are being challenged by the Fe-based amorphous and nanocrystalline alloys which exhibit much higher permeability as well as lower core loss [4]. It has been proved that the low load loss of transformer with amorphous alloy core is only about 1/4 of that with silicon steel cores [5]. The motors with amorphous alloy core can have high speed and energy density much easier [6]. Together with the low energy consumption and high productivity, amorphous alloys and its nanocrystalline derivations are generally acknowledged as double green products for production and application. Moreover, for the deficiencies like bigger size and higher noise of the currently commercial amorphous alloy cores, we can also overcome by developing new alloys with higher properties or by adjusting core design [7]. With the maturity of wide ribbon production, core design, heat treatment, machining technologies, the production and application of amorphous alloys will undoubtedly have rapid growth in the near future.

Great efforts have been devoted to develop new amorphous alloys and optimize the properties by tuning composition,

* Corresponding author. Key Laboratory of Magnetic Materials and Devices, Ningbo Institute of Materials Technology and Engineering, Chinese Academy of Sciences, Ningbo, Zhejiang 315201, China.
E-mail address: ctchang@nimte.ac.cn (C. Chang).

http://dx.doi.org/10.1016/j.jallcom.2015.09.216
0925-8388/

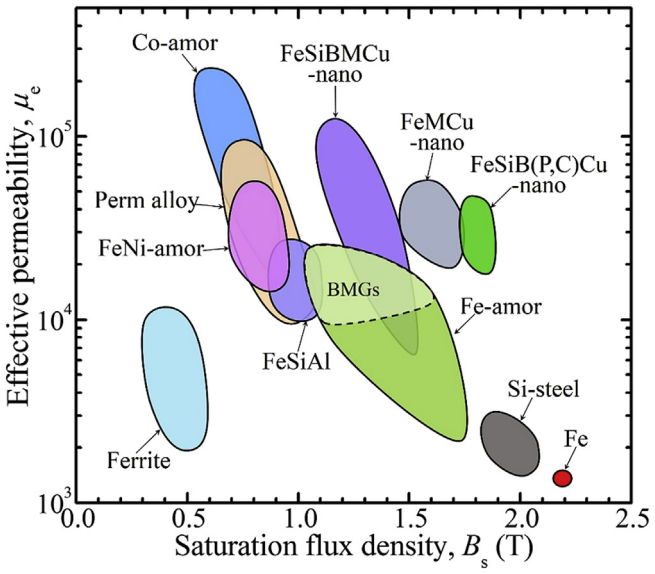

Fig. 1. Relationship between permeability (μ_e) at 1 kHz and saturation flux density (B_s) for soft magnetic materials [17].

production process, heat treatment modes for stress relieving and nanocrystallization since 1967. Many ferromagnetic amorphous alloy systems like FePC [8], FeSiB [9], FePB, FeSiBC [10] as well as Co-based and FeNi-based counterparts [11] were developed for ribbon production and application [12]. As research hotspots in the past two decades, a lot of bulk metallic glasses (BMGs) with high amorphous-forming ability (AFA) and nanocrystalline alloys with good magnetic performance were developed which expanded the application fields and the properties range [13]. However, the obtaining of high AFA for BMGs is always at the expense of the B_s and cost [14]. On the other hand, high B_s amorphous alloys like $Fe_{86}B_7C_7$ and the amorphous precursor of $Fe_{80-85}Si(B,P,C)Cu$ nanocrystalline alloys are hard to be made into wide ribbons by using the current production machine and process, because of the low AFA. Therefore, development of alloys with high B_s and adequate AFA is tremendously desired. Exploring the effects of amorphous forming elements on magnetic properties and AFA of high B_s alloys as well as building composition design rule have great meaning. In addition, since the glass transition and supercooled liquid region for most high Fe content compositions have vanished, the commonly used AFA criterions in BMGs development like ΔT_x, T_{rg} and γ correlated to the T_g are no longer useful [15]. Further investigation is necessary to obtain a reliable and useful criterion to reflect the AFA.

In our recent work, high Fe content $Fe_{83}C_1(Si,B,P)_{16}$ amorphous alloys with excellent magnetic properties and high AFA were successfully developed by introducing new amorphous-forming elements and adjusting composition [16]. Here, the composition design rule for high B_s amorphous alloys is introduced from the binary phase diagram, atomic size and the effects of amorphous forming elements on magnetic performance. The effects of metalloid elements on AFA and magnetic properties as well as origin of the excellent properties are explored.

2. Composition design

Since the amorphous alloys discussed here are developed for wide ribbon production and application, the critical cooling rate and needed AFA are set by the parameters of production machine and planar flow melt spinning process. A new major element selecting rule is used here from the comprehensive consideration of magnetic properties, the cost, the base of AFA need and the mass ribbon manufacturability, different from the former empirical rules for searching compositions likely to yield BMGs [18]. According to the previous reports, most elements on the periodic table shown in Fig. 2 are easily excluded from high B_s Fe-based soft magnetic alloys and the excluding rules are elaborated below.

(1) Gas elements.
(2) Positive or small negative mixing enthalpies with Fe [19].
(3) Precious metal elements.
(4) Element which is prone to form refractory compounds with Fe. Refractory compounds such as oxide inclusions will act as hetero nuclei which will decrease the AFA greatly.
(5) Rare earth elements which have been reported will drastically decrease the B_s and toughness [20,21].
(6) Radioactive element.
(7) Less common element.
(8) Toxic element.
(9) Anti-ferromagnetic element which can improve the anti-corrosion properties will drastically decrease the B_s.

The major element elements of almost all amorphous alloys with high AFA and magnetic properties are shown in Fig. 3. These elements have big negative mixing enthalpies with Fe. According to the relationship between atomic numbers and atomic radius, the alloy systems like FeSiB [9], FePC [8], FeSiBP [14], FeSiB(Nb,Mo,Zr,Y,Ta) [22], FeMoPCB(Si) [23], FeBNbY [20] and FeAlPCB(Si,Ga) [9] meet the atomic size and mixing enthalpy rules for the AFA. It has been pointed out that large (L) and small atoms (S) may form highly packed atomic configuration and reinforced "backbone" structure in the amorphous structure, resulting in the enhancement of the stability of the undercooled liquid, and further suppression of crystallization [24]. On the other hand, the addition of metallic elements with large atomic number will greatly decrease the B_s, by reducing the unfilled 3d orbit of Fe atoms and deteriorating the ferromagnetic exchange interaction by enlarging the distance between magnetic atoms. The addition of Al will increase the melt viscosity and the amount of alumina slag which are really harmful for ribbon production. The most representative ferromagnetic alloy systems are aggregated in the inset of Fig. 3. There were distinctive characteristics in the alloy systems with and without metallic amorphous forming element. As a consequence, it is better for us to select the alloy system without metallic amorphous forming elements for the production of wide ribbon with high B_s.

According to upper analysis, we can have thirteen combinations with Fe, Si, B, P and C. However, the alloys like FeSi and FeC have poor AFA. Only FeB, FeSiB, FeBC [25], FePC [8], FeSiBP [14], FeSiBC and FeSiBPC [26] systems can be made into single amorphous state by melt spinning method. FeSiB and FeSiBC amorphous alloys with high B_s have been widely used with the trademarks of Metglass 2605SA1 and Metglass 2605HB1 [7]. It has been proved that the optimal Fe contents are about 80 and 82 at.% [7] for FeSiB and FeSiBC amorphous alloys, based on the AFA need of planar flow melt spinning process [27]. The FeSiBP and FeSiBPC alloys with Fe content about 76 at.% has been proved have high AFA and could be made into bulk samples in recent years [14,26,28]. In order to develop high B_s amorphous alloys by increasing the Fe content, the FeSiBP and FeSiBPC alloy systems with high AFA are two promising candidates.

The Fe content was selected according to the phase diagrams of Fe–B, Fe–P, Fe–C and Fe–Si shown in Fig. 4. It is clear that the eutectic point of Fe–B, Fe–P, Fe–C are 17%, 17% and 17.1%, respectively. The eutectic point of Fe–Si is higher than 30%. In the full

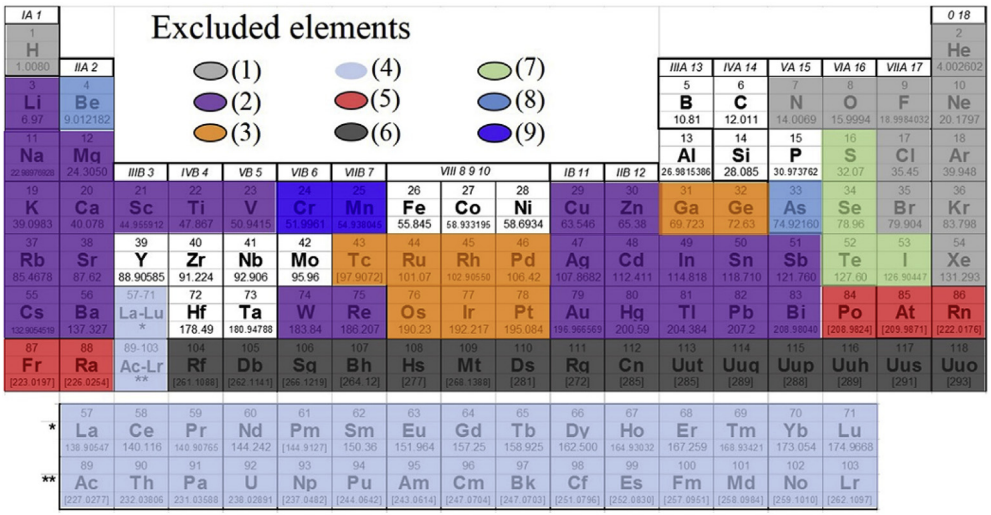

Fig. 2. Selectively excluded elements for high B_s soft-magnetic amorphous alloys.

range of Fe-based amorphous alloys, the Fe and Si are mutually soluble. In addition, the liquidus temperature of eutectic alloys with P and C are lower than that of $Fe_{83}B_{17}$. Therefore, we can speculate that the alloys with 17% amorphous forming elements will exhibit high AFA and B_s. Since the high content addition of P and C will drastically decrease the B_s and change the ribbon production parameters, minor substitution is commonly used for composition revision [29]. In this paper, $Fe_{83}B_{17}$, $Fe_{83}B_{15}Si_2$, $Fe_{83}B_{14}Si_2C_1$, $Fe_{83}B_{12}Si_2P_3$ and $Fe_{83}B_{11}Si_2P_3C_1$ were prepared. The effects of B, Si, P and C on the AFA as well as the magnetic properties are discussed.

3. Experiment procedures

Multicomponent alloy ingots with nominal compositions of $Fe_{83}B_{17}$, $Fe_{83}B_{15}Si_2$, $Fe_{83}B_{14}Si_2C_1$, $Fe_{83}B_{12}Si_2P_3$, $Fe_{83}B_{11}Si_2P_3C_1$ were premelted by induction melting the mixtures of pure Fe (99.99 mass%), crystalline B (99.5 mass%), pre-alloyed Fe–P and Fe–C ingots under a high-purity argon atmosphere. Ribbons with width of about 1 mm and thickness of about 20–100 μm were prepared by single copper roller melt-spinning method. The thickness was controlled by changing the wheel speed. The amorphous structure was identified by X-ray diffraction (XRD) with Cu Kα radiation. Thermal physical parameters including Curie temperature (T_c) and crystallization temperature (T_x) of the amorphous alloys were examined by differential scanning calorimetry (DSC) at a heating rate of 0.67 K/s. The liquidus temperature (T_l) was measured with a DSC by cooling the molten alloy samples at a low cooling rate of 0.067 K/s to reduce the influence of undercooling. As the magnetic properties depend on the sample sizes, in the interest of clarification the intrinsic soft-magnetic properties of this amorphous alloy system, ribbon samples with similar size mentioned above were used for measurement. Saturation flux density (B_s) under a maximum applied field of 800 kA/m was measured with a vibrating sample magnetometer (VSM). Coercivity (H_c) was measured with a DC B–H loop tracer under a field of 800 A/m. Effective permeability (μ_e) at 1 kHz was measured with an impedance analyzer under a field of 1 A/m. All of the ribbon samples for magnetic property measurements were annealed for 1 h in order to reduce the influence of inner stress on soft-magnetic properties through structural relaxation. The density was measured by the Archimedean method. All the measurements were performed at room temperature.

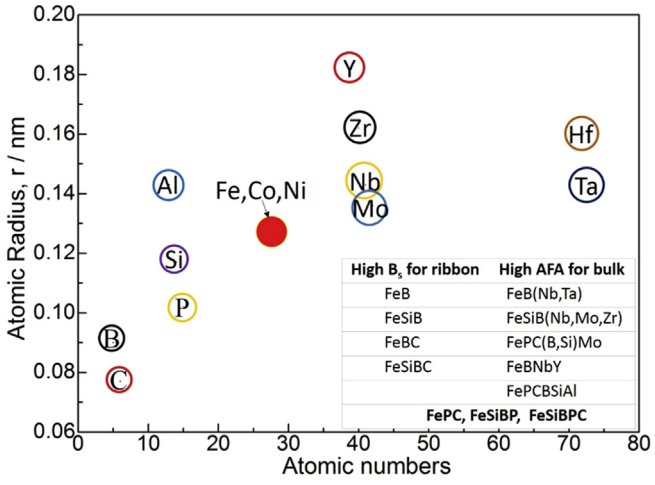

Fig. 3. Relationship between atomic numbers and atomic radius of commonly used elements in amorphous soft-magnetic alloys.

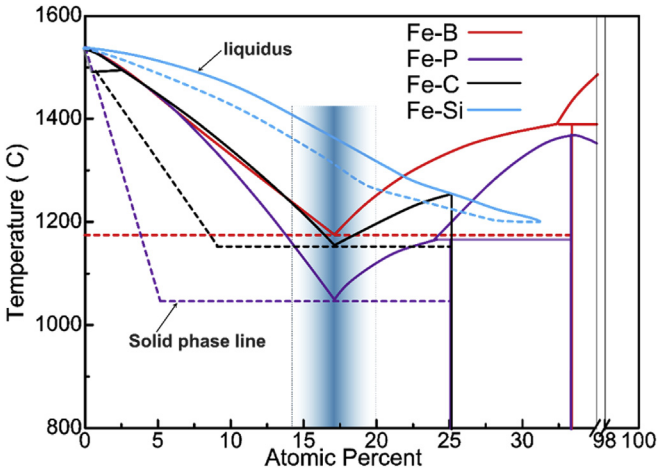

Fig. 4. Binary phase diagrams of Fe–B, Fe–P, Fe–C and Fe–Si.

4. Result and discussion

Fig. 5 shows DSC curves obtained from the $Fe_{83}B_{17-a-b-c}Si_aP_bC_c$ master alloys. The heating rate of the melting process and the cooling rate of the solidification process are commonly used 0.67 K/s and 0.067 K/s, respectively. The onset and off-set temperatures of the melting endothermic event shown in the heating section were designated by T_m and T_{lm}. The onset temperature of the solidification exothermic event shown in the cooling section is designated by T_{ls}. With the addition of Si_2, Si_2C_1, Si_2P_3 and $Si_2P_3C_1$, T_m and T_{lm} decrease gradually. The fusion enthalpies obtained from the area of the fusion peak in DSC data decrease clearly, which indicates the lower binding energy of the crystalline phases. As can be seen from the solidification curves, the crystallization peak splits with the increase of Si implies the diversity of precipitation phases. In addition, it is clear that the changes of T_m, T_{lm} and T_{ls} show different trends. As the solidification process is quasi-static because of the low cooling rate, T_{ls} reflect the liquidus temperature and undercooling. The undercooling determined by the $T_{lm}-T_{ls}$ of the Si_2, Si_2C_1, Si_2P_3 and $Si_2P_3C_1$ doped alloys decreases which can be related to the structure differences between the liquid and primary solid phases.

Single roller melt-spinning method was used to evaluate the AFA of these alloys. Ribbon thickness was controlled by changing the wheel speed. The critical thickness and wheel speed were selected as the indexes of AFA. In order to decrease the errors, all experiments with critical wheel speed were performed at least three times. Fig. 6 shows the XRD patterns taken from the free surface of melt-spun $Fe_{83}B_{17}$, $Fe_{83}B_{15}Si_2$, $Fe_{83}B_{14}Si_2C_1$, $Fe_{83}B_{12}Si_2P_3$ and $Fe_{83}B_{11}Si_2P_3C_1$ alloy ribbons with critical thickness. The XRD patterns exhibit only diffuse halos, and no sharp diffraction peaks corresponding to crystalline phases are visible. It is clear that the AFA increase clearly with the addition of Si, C and P. $Fe_{83}B_{12}Si_2P_3$ and $Fe_{83}B_{11}Si_2P_3C_1$ alloy exhibit high AFA and can be made into single amorphous phase by using the common speed (18–25 m/s) of wide ribbon production. This result confirms the effectiveness of composition design rules for Fe-based amorphous alloys we described in part 2.

In order to investigate the effect of B, Si, C and P on the properties of high Fe content amorphous alloys, we choose the alloy ribbons made with wheel speed higher than critical values except the $Fe_{83}B_{17}$. $Fe_{83}B_{15}Si_2$, $Fe_{83}B_{14}Si_2C_1$, $Fe_{83}B_{12}Si_2P_3$ and $Fe_{83}B_{11}Si_2P_3C_1$ alloy ribbons made with 35 m/s were used. All of the melt-spun ribbons used for thermal and magnetic tests confirmed in the X-ray diffraction patterns are composed of a full amorphous phase without crystallization. Fig. 7 shows the DSC curves exhibiting the crystallization behavior of the $Fe_{83}B_{17-a-b-c}Si_aP_bC_c$ amorphous alloys. No obvious glass transition can be detected for all alloys. As enlarged in the inset, T_c increase with the addition of Si and C, and decrease with the addition of P. All alloys exhibit lower T_c compared with that of the commercial FeSiB and FeSiBC alloys [16]. In addition, the $Fe_{83}B_{17}$ amorphous alloy exhibits only one sharp crystallization exothermic peak. The Si added amorphous alloys have two exothermic peaks. As shown in the enlarged DSC figure, the exothermic peaks of the $Fe_{83}B_{12}Si_2P_3$ and $Fe_{83}B_{11}Si_2P_3C_1$ amorphous alloys are wider than that of the other one. Accordingly, we can speculate that the precipitation phases of the Si added alloys are more complicated. The crystallization rate of the

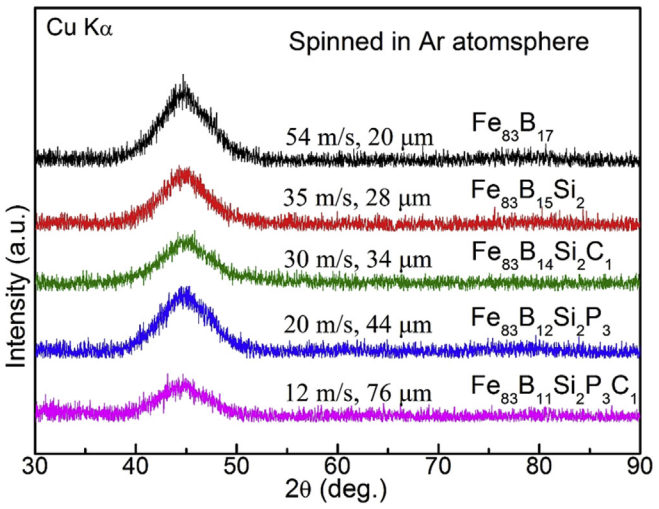

Fig. 6. XRD patterns of the $Fe_{83}B_{17-a-b-c}Si_aP_bC_c$ amorphous alloys with critical thickness.

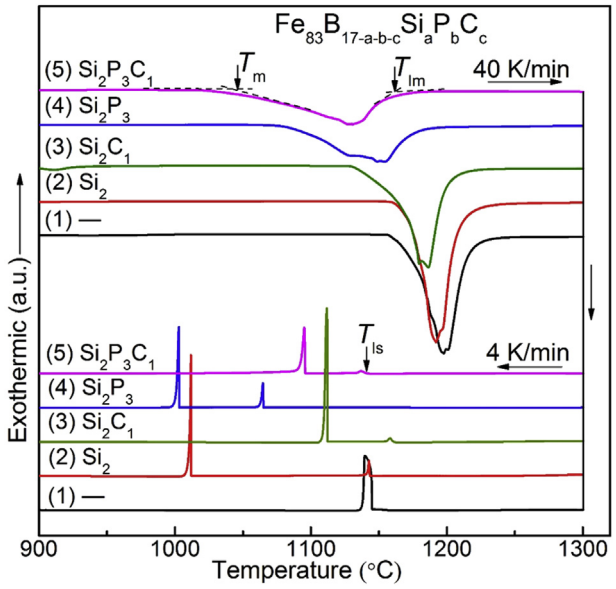

Fig. 5. DSC curves of the $Fe_{83}B_{17-a-b-c}Si_aP_bC_c$ master alloys showing the melting and solidification processes.

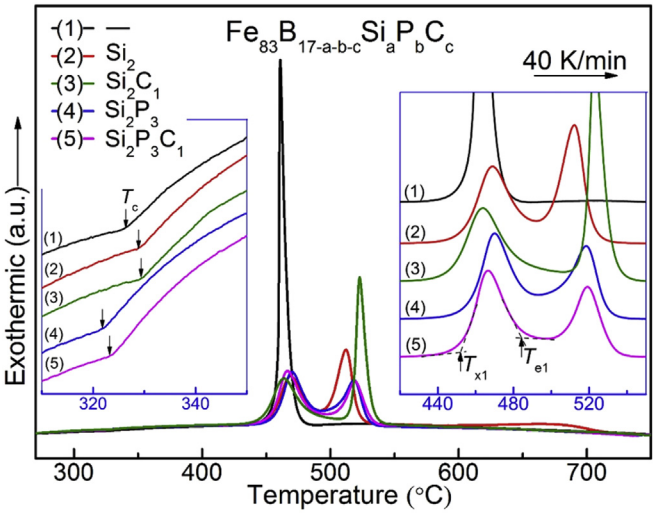

Fig. 7. DSC curves of the $Fe_{83}B_{17-a-b-c}Si_aP_bC_c$ amorphous alloys showing the crystallization behavior.

$Fe_{83}B_{12}Si_2P_3$ and $Fe_{83}B_{11}Si_2P_3C_1$ amorphous alloys are slower. Since the T_{x1} do not changes clearly, all alloys with high Fe content exhibit the advantages of low T_c and large T_{x1}-T_c which indicates a lower annealing temperature and large annealing temperature range [16].

Magnetic properties of the $Fe_{83}B_{17-a-b-c}Si_aP_bC_c$ amorphous alloys subjected to stress relief annealing are investigated systematically. Table 1 summarizes the thermal stability and magnetic thermal parameters, magnetic properties, critical wheel speed and thickness of the $Fe_{83}B_{17-a-b-c}Si_aP_bC_c$ amorphous alloys. Only slight changes of B_s can be detected. All alloys exhibit a high B_s. It is noted that the soft magnetic properties changes greatly. The H_c of $Fe_{83}B_{15}Si_2$, $Fe_{83}B_{14}Si_2C_1$, $Fe_{83}B_{12}Si_2P_3$ and $Fe_{83}B_{11}Si_2P_3C_1$ alloys are much lower than that of the $Fe_{83}B_{17}$. The low H_c and high effective permeability (μ_e) at 1 kHz of alloys with high AFA confirms the high amorphicity and stability of phase. Hence, we can also draw a conclusion that excellent soft magnetic properties can be gained, so long as we meet the needed AFA when developing new Fe-based amorphous alloys.

It is now well established that amorphous formation in metallic liquids is essentially a competing process between liquid phases and the crystalline phases [30]. Any factors which can increase liquid phase stability or suppress crystallization would enhance the AFA. In order to investigate the effect of Si, P and C addition on the crystallization process and thermal stability of the amorphous phase, XRD measurements were carried out for the alloy ribbons with as-quenched and annealed state. Fig. 8 shows the XRD patterns of the as-quenched samples prepared with wheel speed lower than the critical values. The precipitated phases of the $Fe_{83}B_{17}$ alloy are Fe_3B and Fe_2B. For the alloys with Si addition, the Fe_2B is suppressed and α-Fe(Si) shares the maximum proportion. In addition, the Fe_3B transforms to Fe_3(B,P) for the P containing alloys, implying that the lattice parameters enlarges and some B atoms are substituted by P atoms. Since Fe_3(B,P) contains three different elements and its structure is more complex, the crystallization process requires longer range atom rearrangements of constituent elements. As proved, the precipitation of α-Fe(Si) phase always undergoes competing process [31]. All of these will increase the thermal stability of molten alloy and the AFA.

Fig. 9 shows the XRD patterns of the $Fe_{83}B_{17}$, $Fe_{83}B_{11}Si_2$ and the $Fe_{83}B_{11}Si_2P_3C_1$ alloy ribbons annealed at 440 °C for 10 min. For the $Fe_{83}B_{17}$ alloys without Si, the only eutectic peak is identified to correspond to the precipitation of α-Fe(Si) and Fe_2B. For the $Fe_{83}B_{11}Si_2$ and the $Fe_{83}B_{11}Si_2P_3C_1$ alloys, the primary phase is identified as α-Fe(Si). All the results show that the introduction of Si stimulates the precipitation of α-Fe(Si) crystals and depress the formation of Fe_2B and Fe_3(B, P) which have been verified as hard-magnetic phases. The formation of fine α-Fe(Si) phases or clusters without other phases is good for the soft-magnetic properties [32]. Together with the high AFA, it is easy to understand the excellent magnetic performance of the Si containing alloys.

First, we discuss the effects of metalloid elements on magnetic properties. The improvement of soft-magnetic properties including H_c and μ_e can be explained from the aspects of increasing AFA and

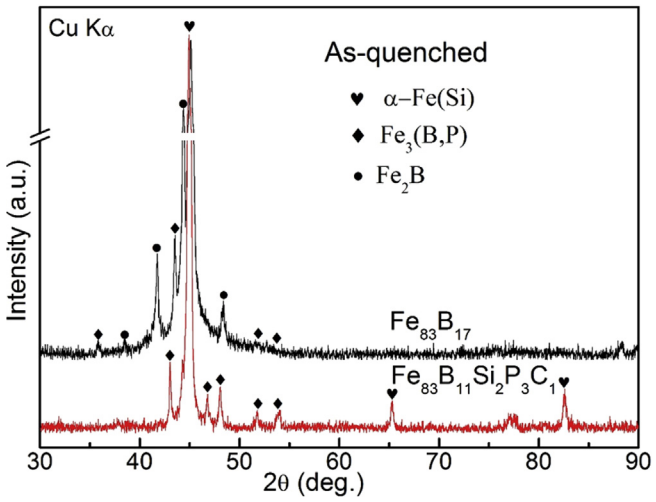

Fig. 8. XRD patterns of the $Fe_{83}B_{17}$ and the $Fe_{83}B_{11}Si_2P_3C_1$ alloy ribbons spinned with wheel speed lower than the critical values.

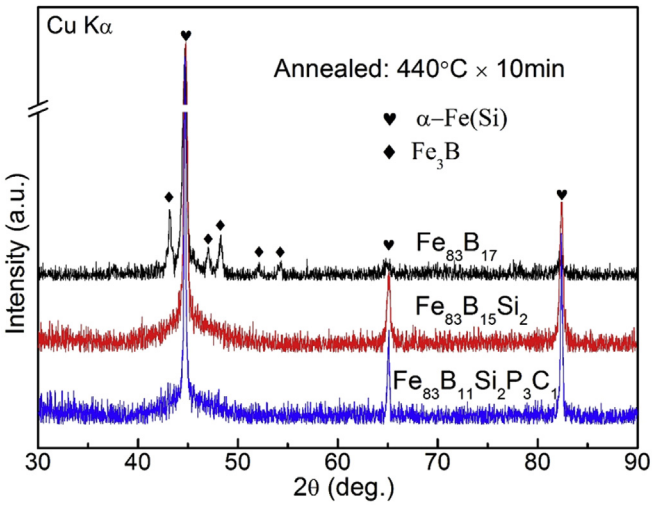

Fig. 9. XRD patterns of the $Fe_{83}B_{17}$, $Fe_{83}B_{11}Si_2$ and the $Fe_{83}B_{11}Si_2P_3C_1$ alloy ribbons annealed at 440 °C for 10 min.

transformation of primary phase to α-Fe(Si). Bitoh et al. has found the alloy system with high AFA will result in high degree of amorphicity and structural homogeneity which may act as quasi-dislocation dipoles (QDDs) and domain-wall pinning sites [33]. As shown in Fig. 7, T_c increases with the addition of Si and C, and decreases with the addition of P. This fact implies that the T_c of Fe-based amorphous alloys cannot be explained only by the simple charge transfer model and it is necessary to consider other factors such as the size of metalloid atoms and the short-range order

Table 1
Thermal parameters, magnetic properties, critical wheel speed and thickness of the $Fe_{83}B_{17-a-b-c}Si_aP_bC_c$ amorphous alloys.

Constitution		Thermal properties					AFA		Magnetic properties		
		T_c (°C)	T_{x1} (°C)	T_m (°C)	T_{lm} (°C)	T_{ls} (°C)	V_c (m/s)	T_m (μm)	B_s (T)	H_c (A/m)	μ_e
1	$Fe_{83}B_{17}$	325	459	1175	1214	1156	54	20	1.65	18	3400
2	$Fe_{83}B_{15}Si_2$	327	453	1175	1207	1143	35	28	1.68	3.0	8100
3	$Fe_{83}B_{12}Si_2C_1$	328	447	1132	1199	1161	35	29	1.67	4.2	7600
4	$Fe_{83}B_{12}Si_2P_3$	322	457	1092	1173	1065	20	44	1.66	1.9	8700
5	$Fe_{83}B_{11}Si_2P_3C_1$	323	454	1036	1155	1141	12	76	1.67	2.1	10,300

variations. In Fe-based alloys, B and P atom are prone to form compounds or short-range order with Fe. Si and C atom are interstitial atoms. The substitution of B by P will enlarge the distance of the Fe atoms which can also be proved by the change of density. The substitution of B by Si and C will decrease the distance of the Fe atoms which will lead to increase of exchange coupling interaction. The magnetic moment changes with adding of P, Si and C can be interpreted from the number of electron transfer from metalloid atom to 3d shell of Fe atom. For B, C, Si and P, the outermost electrons are $2p^1$, $2p^2$, $3p^2$ and $3p^3$, respectively. The B_s of the alloys in this work does not change clearly due to the minor addition.

Then we explore the mechanism of the increase of AFA. The reasons are as follows: (1)According to the composition design rule depicted in part 2, the combination of Si, B, P, C and Fe meet the empirical component rules for achievement of high AFA [18]. The mixing enthalpies of Fe and Si, B, P pairs are −18, −11 and −31 kJ/mol, respectively. The C, B, P, Si and Fe have large atomic size mismatches (shown in Fig. 3). The substitution of B by Si, P and C increase the complexity [13,18]. All these will lead to high degree of dense randomly packed atomic configurations and reinforced "backbone" structure in the amorphous structure, resulting in the enhancement of the stability of the undercooled liquid, and further suppresses crystallization. (2)$Fe_{83}B_{17}$, $Fe_{83}B_{15}Si_2$, $Fe_{83}B_{14}Si_2C_1$, $Fe_{83}B_{12}Si_2P_3$ and $Fe_{83}B_{11}Si_2P_3C_1$ alloys were designed according to the two binary phase diagrams in Fig. 4. A deep eutectic point is achieved by combining the Fe–B, Fe–P and Fe–C alloys with similar Fe content, which can be seen from the decreasing T_m, T_{lm} in Fig. 5 [34]. From the thermodynamic viewpoint, the driving force for crystal nucleation and growth below the eutectic temperature is comparatively small. (3) With the substitution of Si, the primary phase transforms from Fe_2B to α-Fe(Si) which can increase the competing effect. In addition, the addition of P and C make the boride precipitation phase more complexity.

5. Conclusion

According to the composition design rules from the binary phase diagram, atomic size and the effects of amorphous forming elements on magnetic performance, high B_s amorphous alloy systems containing FeB, FeSiB, FeSiBP, FeSiBC and FeSiBPC are designed. The Fe content is determined as 83 at% in the light of the similar Fe content of Fe–B, Fe–P and Fe–C eutectic alloys. The alloy systems with the combination of Fe, B, P, C and Si is beneficial to the achievement of high B_s and AFA. The effects of metalloid elements on AFA and magnetic properties as well as origin of the excellent properties are explored. With the addition of Si, P and C in $Fe_{83}B_{17}$, the critical wheel speed decrease from 54 m/s to 12 m/s and the maximum thickness increase to 76 μm. The improvement of the AFA is owing to the competition effect of the α-Fe(Si) precipitation and the approach of deep eutectic point. The excellent soft-magnetic properties are attributed to the high degree of amorphicity and structural homogeneity.

Acknowledgments

This work was supported by the National Scientific and Technological Support Projects No. 2013BAE08B01. National Natural Science Foundation of China (Grant No. 51201174).

References

[1] O. Gutfleisch, M.A. Willard, E. Brück, C.H. Chen, S.G. Sankar, J.P. Liu, Adv. Mater. 23 (2011) 821–842.
[2] K. Suzuki, G. Herzer, in: D. Sellmyer, R.Skomski (Eds.), Springer, New York, 2006, p. 365 (Chapter 13).
[3] A.M. Leary, P.R. Ohodnicki, M.E. McHenry, JOM 64 (2012) 772–781.
[4] R. Hasegawa, J. Magn. Magn. Mater. 304 (2006) 187–191.
[5] R. Hasegawa, Mater. Sci. Eng. A 375 (2004) 90–97.
[6] D.K. Hong, D. Joo, B.C. Woo, Y.H. Jeong, D.H. Koo, IEEE Trans. Magn. 49 (2013) 4072–4075.
[7] Y. Ogawa, M. Naoe, Y. Yoshizawa, R. Hasegawa, J. Magn. Magn. Mater. 304 (2006) E675–E677.
[8] J.F. Wang, R. Li, N.B. Hua, L. Huang, T. Zhang, Scr. Mater. 65 (2011) 536–539.
[9] A. Inoue, A. Katsuya, K. Amiya, T. Masumoto, Mater. Trans. JIM 36 (1995) 802–809.
[10] D. Azuma, R. Hasegawa, IEEE Trans. Magn. 47 (2011) 3460–3462.
[11] A.D. Wang, M.X. Zhang, J.H. Zhang, H. Men, B.L. Shen, S.J. Pang, T. Zhang, J. Alloys Compd. 536 (2012) S354–S358.
[12] A. Inoue, A. Takeuchi, Acta Mater. 59 (2011) 2243–2267.
[13] D.V. Louzguine-Luzgin, A. Inoue, in: K.H.J. Buschow (Ed.), Handbook of Magnetic Materials, 21, Elsevier, 2013, pp. 131–171 (Chapter 3).
[14] A. Makino, T. Kubota, M. Makabe, C. Chang, A. Inoue, Mater. Sci. Forum 1361 (2007) 561–565.
[15] Z.P. Lu, C.T. Liu, Phys. Rev. Lett. 91 (2003) 115505.
[16] A.D. Wang, C.L. Zhao, H. Men, A.N. He, C.T. Chang, X.M. Wang, R.W. Li, J. Alloys Compd. 630 (2015) 209–213.
[17] A. Makino, T. Hatanai, A. Inoue, T. Masumoto, Mater. Sci. Eng. A 226 (1997) 594–602.
[18] A. Inoue, Acta Mater. 48 (2000) 279–306.
[19] A. Takeuchi, A. Inoue, Mater. Trans. 46 (2005) 2817–2829.
[20] C.Y. Lin, M.C. Lee, T.S. Chin, J. Phys. D. Appl. Phys. 40 (2007) 310–314.
[21] T.A. Baser, M. Baricco, J. Alloys Compd. 434 (2007) 176–179.
[22] A. Inoue, B.L. Shen, Adv. Mater. 16 (2004) 2189–2192.
[23] F.J. Liu, S.J. Pang, R. Li, T. Zhang, J. Alloys Compd. 483 (2009) 613–615.
[24] D.B. Miracle, W.S. Sanders, O.N. Senkov, Philos. Mag. 83 (2003) 2409–2428.
[25] S. Hatta, T. Egami, C.D. Graham, Appl. Phys. Lett. 34 (1979) 113–115.
[26] A. Makino, C.T. Chang, T. Kubota, A. Inoue, J. Alloys Compd. 483 (2009) 616–619.
[27] A. Makino, H. Men, K. Yubuta, T. Kubota, J. Appl. Phys. 105 (2009) 013922.
[28] C.T. Chang, T. Kubota, A. Makino, A. Inoue, J. Alloys Compd. 473 (2009) 368–372.
[29] C.D. Graham, T. Egami, IEEE Trans. Magn. 15 (1979) 1398–1403.
[30] P. Jalali, M. Li, Intermetallics 12 (2004) 1167–1176.
[31] H.X. Li, J.E. Gao, Y. Wu, Z.B. Jiao, D. Ma, A.D. Stoica, X.L. Wang, Y. Ren, M.K. Miller, Z.P. Lu, Sci. Rep. 3 (2013).
[32] G. Herzer, Acta Mater. 61 (2013) 718–734.
[33] T. Bitoh, A. Makino, A. Inoue, J. Appl. Phys. 99 (2006), 08F102.
[34] G.J. Hao, Y. Zhang, J.P. Lin, G.L. Chen, Rev. Adv. Mater. Sci. 18 (2008) 159–163.